SPECIAL ISSUE

Coupled THM processes in EDZ of crystalline rocks using an elasto-plastic cellular automaton

Peng-Zhi Pan · Xia-Ting Feng · Xiao-Hua Huang · Qiang Cui · Hui Zhou

Abstract This paper aims at a numerical study of coupled thermal, hydrological and mechanical processes in the excavation disturbed zones (EDZ) around nuclear waste emplacement drifts in fractured crystalline rocks. The study was conducted for two model domains close to an emplacement tunnel; (1) a near-field domain and (2) a smaller wall-block domain. Goodman element and weak element were used to represent the fractures in the rock mass and the rock matrix was represented as elasto-visco-plastic material. Mohr–Coulomb criterion and a non-associated plastic flow rule were adopted to consider the viscoplastic deformation in the EDZ. A relation between volumetric strain and permeability was established. Using a self-developed EPCA^{2D} code, the elastic, elasto-plastic and creep analyses to study the evolution of stress and deformations, as well as failure and permeability evolution in the EDZ were conducted. Results indicate a strong impact of fractures, plastic deformation and time effects on the behavior of EDZ especially the evolution of permeability around the drift.

Keywords DECOVALEX-THMC · EPCA^{2D} · EDZ · Crystalline rock · Fracture network

P.-Z. Pan · X.-T. Feng (✉) · X.-H. Huang · H. Zhou
State Key Laboratory of Geomechanics and Geotechnical
Engineering, Institute of Rock and Soil Mechanics, Chinese
Academy of Sciences, 430071 Wuhan, China
e-mail: xtfeng@whrsm.ac.cn

Q. Cui
Northeastern University, Shenyang
110004, Liaoning, China

Introduction

The thermo-hydro-mechanical and chemical (THMC) processes (Tsang 1987) in rocks are increasingly important research topics, mainly due to the demands for the design, construction, operation and performance/safety assessments of underground radioactive waste repositories and other civil and environmental engineering works such as dam foundations, slopes, underground storage caverns and geothermal energy extraction. Extensive research on fundamental aspects of coupled THMC processes for nuclear waste disposal in subsurface have been conducted in international co-operation projects in the world, with the typical example of the international DECOVALEX (DEvelopment of COupled models and their VALidation against EXperiments) project series (Stephansson et al. 1996; Stephansson et al. 2004; Hudson et al. 2005; Hudson and Christiansson 2006). This paper represents a work performed for Task B of the DECOVALEX-THMC (2004–2007) (Tsang et al. 2008).

As far as the THMC experiments and mathematical model are concerned, Hart and John (1986) built a fully coupled THM model for non-linear geologic system. Noorishad et al. (1984) studied the coupled THM phenomena in saturated fractured porous rocks. Nguyen and Selvadurai (1995) studied the impact of THM processes on nuclear and fuel waste disposal, based on Biot's theory of poroelasticity. Feng et al. (2001, 2004) studied the effects of water chemistry on micro-cracking and compressive strength of granite using a meso-mechanical experimental system. Both laboratory and field experiments related to THMC coupling have been reported extensively in the literature (Elsworth 2003; Polak et al. 2004; Liu et al. 2006; Elsworth and Yasuhara 2006; Yasuhara and Elsworth 2006a, b).

In numerical modeling, Jing and Feng (2003) conducted a comprehensive summary of the recent progress in numerical modeling for coupled THMC processes of geological media. The solution of the coupled sets of conservation equations can use either continuum or discrete approaches such as finite element method (FEM), boundary element method (BEM), finite difference method (FDM), finite volume method (FVM) and DEM codes (e.g. Ohnishi et al. 1987; Shen and Stephansson 1993; Noorishad and Tsang 1996; Rutqvist et al. 2001, 2002; Feng et al. 2006a).

However, there are still challenges in understanding the fundamentals of THM coupling in rock matrix and fractures, especially the issues such as representation of fracture networks and EDZ, characterization of the permeability variations of EDZ. Furthermore, the timescales considered for nuclear waste disposal are of the scale of 10^5 years. The solution of these issues depends on realistic representation of fractures or fracture networks, their constitutive models and properties, and a software platform which can conveniently incorporate the governing equations, physical models, engineering measures and initial boundary conditions.

In this paper, Goodman element model and weak element model were used to represent the fractures in the rock mass. Based on the stress and strain states as well as the failure pattern in EDZ of a crystalline rock, a volumetric strain versus permeability relationship was proposed to study the permeability variation of crystalline rocks. The code, EPCA^{2D}, serves as the platform based on the principles of cellular automaton.

The main concept of the EPCA method can be found in Feng et al. (2006a). This code has been successfully used to simulate the failure process of heterogeneous rocks with and without consideration of hydro-mechanical coupling effect (Feng et al. 2006a; Pan et al. 2006a, b). By using this code, detailed analysis of linear elastic, elasto-plastic and creep behavior in rocks over long time for Task B of DECOVALEX-THMC project was conducted. The comparisons of the simulation results between international groups can be found in Bäckström et al. (2008), and the two accompanying papers in this issue by Hudson et al. (2008) and Rutqvist et al. (2008a).

Problem description

This study concerns a hypothetical nuclear waste repository in a granitic rock formation at a depth of 500 m (Rutqvist et al. 2006a, 2008a) (Fig. 1). Two model domains, wall block and near-field model domains, are considered for detailed analysis of coupled THMC

processes in the EDZ of a drift. For these two model domains, two cases are considered:

(1) homogeneous, isotropic rock (no fractures) and
(2) heterogeneous, anisotropic and fractured rock (with various degrees of fractures).

The near-field fracture network model (Fig. 1b) was derived from fracture mapping at the Äspö Hard Rock Laboratory in Sweden. The extraction of the fracture pattern and other relevant data are presented in detail in Bäckström (2006).

Figure 2 presents boundary conditions and interior conditions used to reproduce the coupled THM environment in the wall block and near-field model domains. These boundary and interior conditions were derived from a separate large scale analysis (Rutqvist et al. 2008b). Because these two model domains represent the situation very close to the surface of the drift, the problem is simplified to assume uniform thermal and hydrological conditions over the entire model. Also, an assumption is made that the relative humidity within the entire near-field model domain is in equilibrium.

The initial pre-excavation conditions are represented by in situ stresses, temperature and fluid pressure at a depth of 500 m, with an initial vertical stress of 13.2 MPa, a horizontal stress of 32.1 MPa, a temperature of 25°C, and a fluid pressure of 5.0 MPa.

Model and parameters

The present work focuses on mechanical changes, permeability variation and thermal expansion effect in the EDZ. Heat transfer and fluid flow is not considered. But the evolution of thermal and hydraulic condition is considered for its effect on the evolution of mechanical behavior of EDZ. The EPCA model was extended to include an effective stress formulation to consider the effect of fluid pressure, and a thermal strain formulation to consider effect of temperature. To consider the time effects, the EPCA model was extended to consider creep processes, in which the time dependency may be a function of temperature, water saturation and chemical potential. By introducing a relation between stress/strain and permeability in EPCA model, the permeability variation of rock mass induced by stress was investigated.

Elasto-plastic constitutive relation of cell element

The constitutive relations of an isotropic linear poroelastic medium can be expressed in terms of the effective stress σ'_{ij}

Fig. 1 Two model domains considered for detailed analysis of coupled THMC processes in the EDZ of a drift (Rutqvist et al. 2006a)
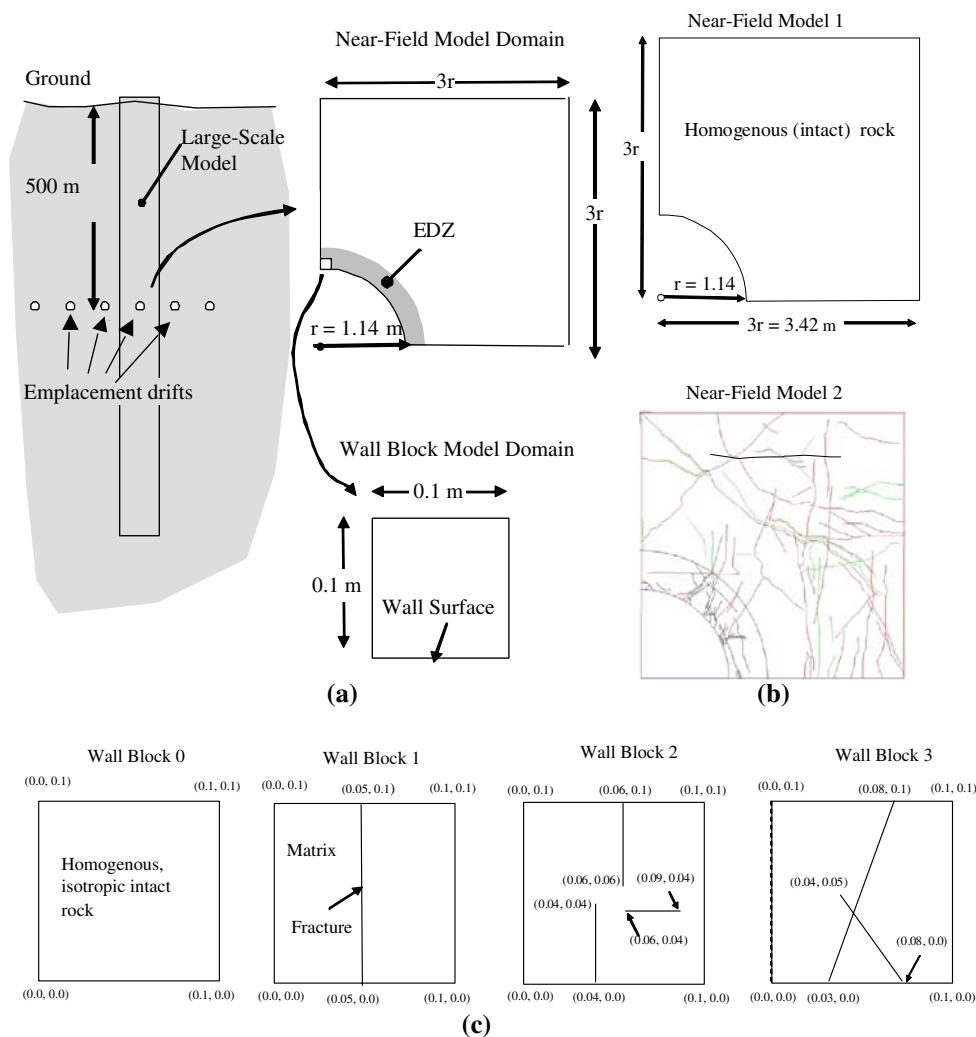
(positive for tension), strain ε_{ij} and temperature change ΔT as (Lewis and Schrefler 1987)

$$\sigma'_{ij} = 2G\left(\varepsilon_{ij} + \delta_{ij}\frac{v}{1-2v}\varepsilon_{kk}\right) - K'\alpha\Delta T\delta_{ij}, \tag{1}$$

where $\sigma'_{ij} = \sigma_{ij} - \xi p\delta_{ij}$ and σ_{ij} is the total stress (positive for tension), δ_{ij} is the Kronecker's delta, p is the pore water pressure, $\xi(\leq 1)$ is a coefficient which depends on the compressibility of the constituents. In the present work, $\xi = 1$ was assumed.

For a perfect elasto-plastic material, the constitutive model between stress and strain, in an increment form, is,

$$d\sigma_{ij} = [D_e]\left(d\varepsilon_{ij} - d\varepsilon_{ij}^p\right) = [D_e]\left(d\varepsilon_{ij} - d\lambda\frac{\partial Q}{\partial \sigma_{ij}}\right). \tag{2}$$

When yield function $F(\sigma) = 0$, the following expression can be obtained,

$$dF = \frac{\partial F}{\partial \sigma_{ij}}d\sigma_{ij} = 0. \tag{3}$$

Substitute Eq. 2 into Eq. 3, Eq. 3 can be expressed as,

$$\left\{\frac{\partial F}{\partial \sigma}\right\}^T[D_e]\{d\varepsilon\} - \left\{\frac{\partial F}{\partial \sigma}\right\}^T[D_e]d\lambda\left\{\frac{\partial Q}{\partial \sigma}\right\} = 0. \tag{4}$$

Thus,

$$d\lambda = \frac{\left\{\frac{\partial F}{\partial \sigma}\right\}^T[D_e]\{d\varepsilon\}}{\left\{\frac{\partial F}{\partial \sigma}\right\}^T[D_e]\left\{\frac{\partial Q}{\partial \sigma}\right\}}. \tag{5}$$

Substitute 5 into 2, the plasticity matrix is expressed as,

$$[D_p] = \frac{\left\{\frac{\partial F}{\partial \sigma}\right\}^T[D_e][D_e]\left\{\frac{\partial Q}{\partial \sigma}\right\}}{\left\{\frac{\partial F}{\partial \sigma}\right\}^T[D_e]\left\{\frac{\partial Q}{\partial \sigma}\right\}}. \tag{6}$$

In Eqs. 2–6, Q is the plastic potential function, F is the yield function, $d\varepsilon_{ij}^p$ is the plastic strain increment tensor, $d\varepsilon_{ij}$ is the strain increment tensor. $[D_e]$ and $[D_p]$ are the elastic and plastic matrices, respectively. $d\lambda$ is a proportional coefficient.

Fig. 2 **a** Derivation of boundary and interior conditions from a large-scale model. **b** Evolution of temperature, fluid pressure, and stresses applied to near-field and wall-block model domains (Rutqvist et al. 2006a, 2008a)
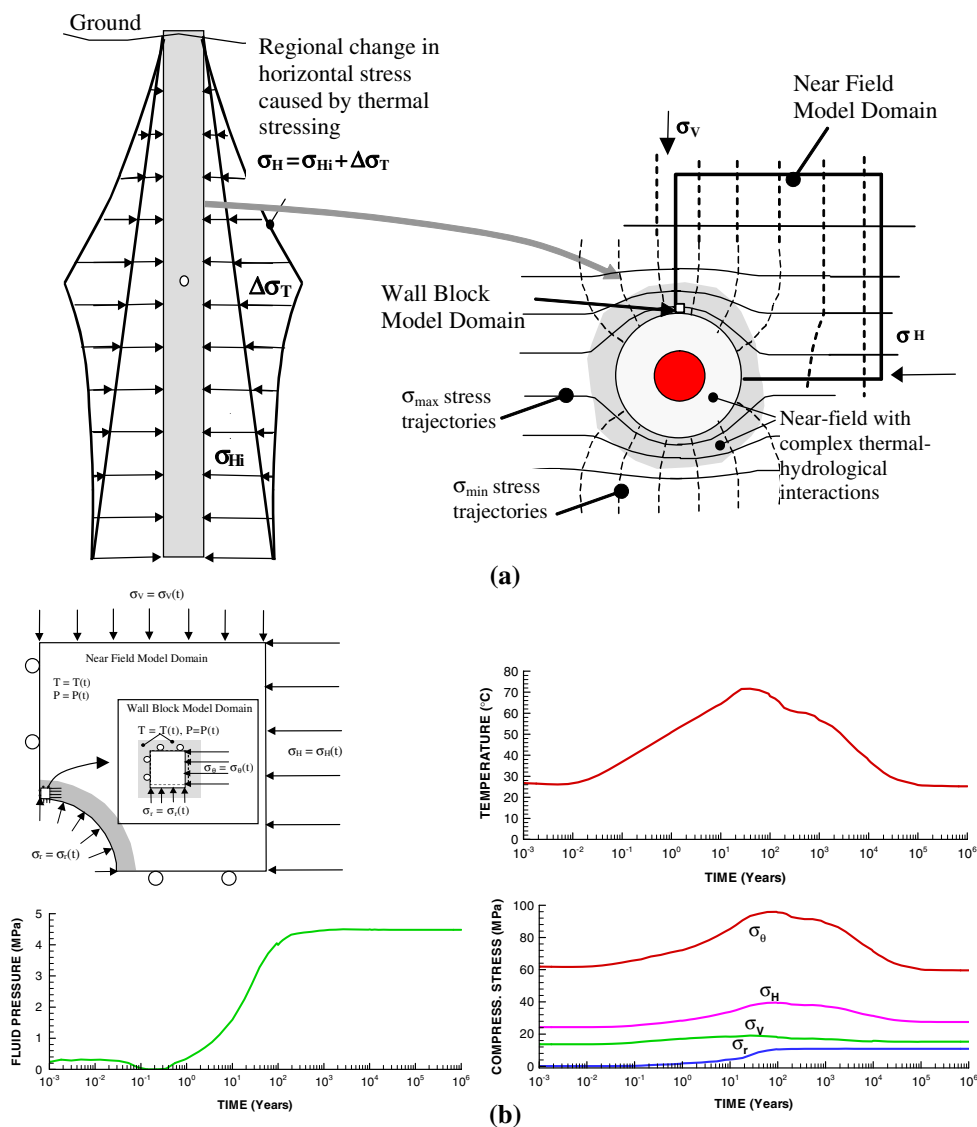
Visco-elasto-plastic models and parameters for intact rock and fractures

In the present work, the following elasto-visco-plastic constitutive relation to model creep behavior of fractured crystalline rock mass was used,

$$\dot{\varepsilon} = D_{e}^{-1}\dot{\sigma} + \alpha \dot{\Delta T} + \Gamma\left\langle \left(\frac{F}{F_0}\right)^N \right\rangle \frac{\partial F(\sigma, \Delta T)}{\partial \sigma}, \qquad (7)$$

where $\dot{\varepsilon}$ is the total strain rate, $\dot{\sigma}$ is the effective stress rate, Γ and N are the visco-plastic parameters which can be obtained from shear creep tests (Desai Chandre et al. 1995).

The visco-plastic parameters Γ and N of the intact granite were obtained from triaxial creep tests (Feng et al. 2006b) using the same procedure as in Desai Chandre et al. (1995).

Mohr–Coulomb yield criterion

In the current EPCA model, different yield criterions such as Mohr–Coulomb or Drucker–Prager can be considered. For Task B, Mohr–Coulomb yield criterion was used.

For elasto-plastic analysis, the yield function of the conventional Mohr–Coulomb yield criterion can be expressed as,

$$F(\sigma) = \frac{1}{2}(\sigma_1 - \sigma_3) + \frac{1}{2}(\sigma_1 + \sigma_3)\sin\varphi - c\cos\varphi, \qquad (8)$$

where c and φ are the cohesion and frictional angle, respectively.

Using non-associated plastic flow rules with different yield function and plastic potential function, i.e., $Q \neq F$. In the present work, the plastic potential function is chosen as the same form of yield function, i.e.,

$$Q(\sigma) = \frac{1}{2}(\sigma_1 - \sigma_3) + \frac{1}{2}(\sigma_1 + \sigma_3)\sin\psi - c\cos\psi, \qquad (9)$$

where dilation angle ψ is different as the friction angle used in the yielding function F (see Eq. 8).

Therefore, $\varphi = \psi$ corresponds to the associated plastic flow rule, which means that the volumetric strain expansion is the more significant when the cell element encounters shear failure. Otherwise, the plastic flow is non-associated. When $\psi = 0$, no dilation occurs, which means that the volumetric strain does not change when the cell element fails with in plastic shear.

Permeability

According to the task definition of DECOVALEX-THMC Task B, the influence of hydraulic field on the stress field can be reflected using the effect stress concept. However, the hydraulic properties such as permeability change or fluid flow were not considered. Therefore, if the permeability change due to stress evolution in crystalline rocks is to be studied, the relation between permeability and stress/strain should be developed. One way to do this is to use the data from similar crystalline rock tunnels such as TSX or Mine-by at URL. Based on the in-situ field experiments at URL, Rutqvist (2007) conducted modeling and calibration of near-field rock responses using the combined mean stress and deviatoric stress relation according to

$$k = [k_r + \Delta k_{max}\exp(\beta_3\sigma_m)]\exp(\gamma\Delta\sigma_d) \qquad (10)$$

Reasonable permeability changes in the rock both on the top and side of the TSX tunnel was obtained by using this model for linear elastic solution (Rutqvist et al. 2008c).

In order to develop a model to numerically predict permeability changes induced in EDZ, the permeability change is related to volumetric strain. This is because volumetric strain increases near the spring line of the drift but decreases on the top of the drift where more shear/deviatoric strain occur. If the shear dilation is considered, an increase of volumetric strain also on top of the drift caused by shear dilation can be found. The relation is given as

$$k = k_r + \Delta k_{max}\exp(\beta_2\varepsilon_v), \qquad (11)$$

where, ε_v is the volumetric strain relative to zero mean stress conditions. k_r is the residual permeability if the rock is compressed to a very high mean stress. Δk_{max} is the maximum change in permeability that can be achieved by compressing a rock sample from zero stress to a very high compressive stress. β_2 is a parameter related to volumetric modulus,

$$\beta_2 = \beta K, \qquad (12)$$

where, K is the bulk modulus. β is a parameter that may be used to calibrate this function against some tests of volumetric strain versus permeability.

Table 1 Rock matrix and fracture element properties for elasto-plastic analysis

Parameter	Matrix elements	Fracture elements
Young's modulus, E	70 GPa	X GPa
Poisson ratio, v	0.3	0.3
Cohesion strength, C	15 MPa	1 MPa
Friction angle, ϕ	49°	27°
Dilation angle, d	0–49°	0–27°
Resdidual permeability, k_r	1×10^{-20} m^2	8.3×10^{-16} m^2
Maximum permeability change, Δk_{max}	1.4×10^{-18} m^2	8.3×10^{-13} m^2
Strain-permeability constant, β	4×10^{-8}	4×10^{-8}

If the parameters in Eq. 11 and the dilation angle in the elasto-plastic model were chosen, the changes in permeability can be obtained. In order to consider the effect of shear dilation on the permeability change, different dilation angle values were considered. In the present simulation, part of the parameters is listed in Table 1.

Fracture representations

Fracture representation is very important in the simulation of EDZ evolution. Different models to represent the fractures in the simulation were used. This includes Goodman element and weak element models.

Goodman element

Different Goodman element models were presented in this section, including traditional model and modified model. Figure 3a is the traditional Goodman element model (GJE1), whose normal and shear stiffness are constant during loading processes. Figure 3b is a modified Goodman element model (GJE2), whose normal stiffness is a non-linear function of normal displacement, and shear stiffness is constant. Another modified Goodman element model (GJE3) is shown in Fig. 3c. In particular, GJE3 can consider complex deformation modes of fractures such as opening, slip, sticking, interpenetration and re-contact, which may happen during a creep process.

Weak element

A solid element with reduced mechanical properties was used as another fracture representation. This kind of fracture representation was called as weak element.

For a weak element, the stiffness of the element depends on the size of the element and a simple formula is used for selecting the appropriate Young's modulus for the element, i.e.,

Fig. 3 Schematic representation of two different Goodman elements. **a** The traditional Goodman element (GJE1). **b** Modified Goodman element (GJE2). **c** Modified Goodman element (GJE3)

(a)

(b)

(c)
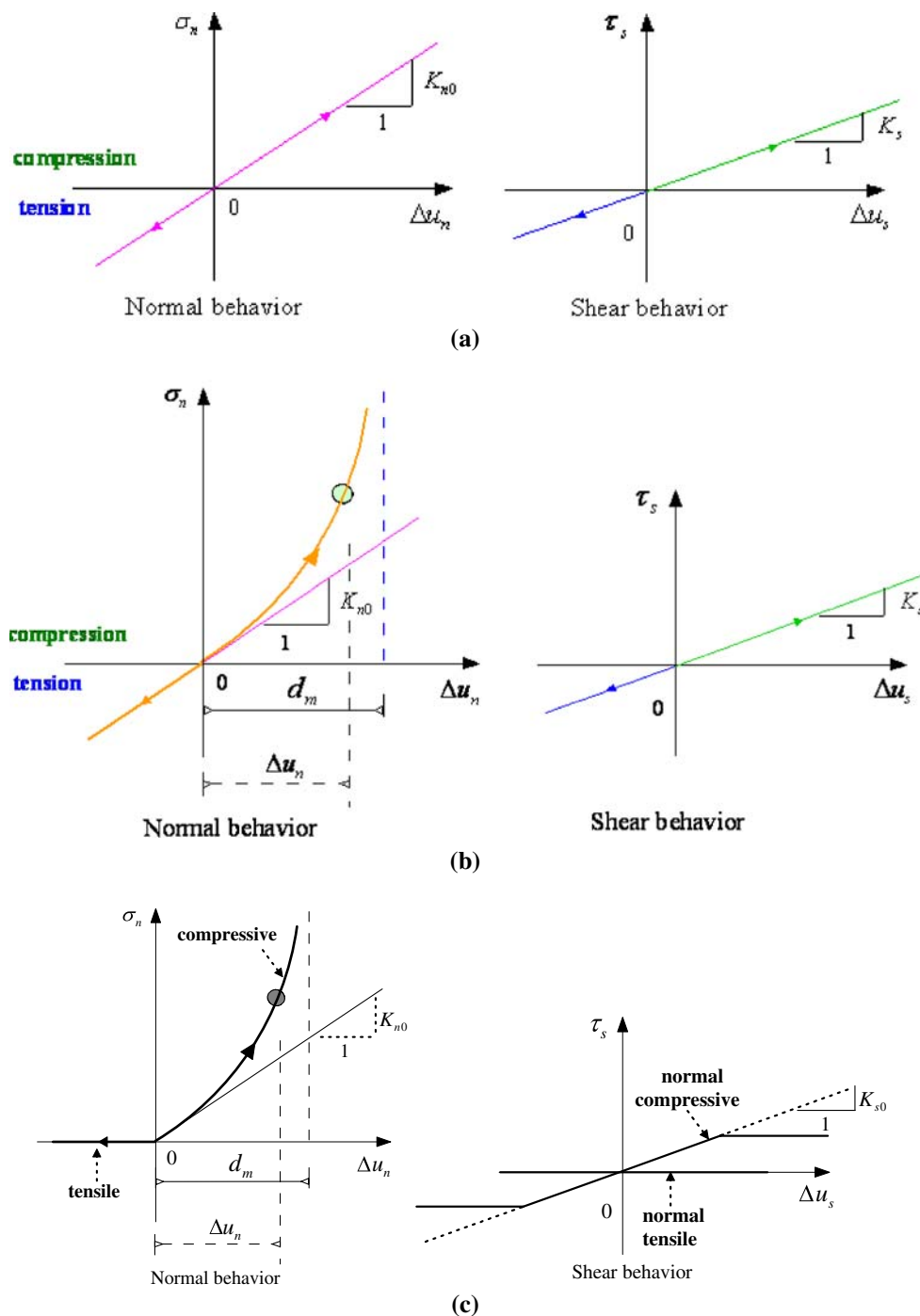
$$\frac{1}{E_j} = \frac{1}{E_r} + \frac{1}{kn \times b}, \tag{13}$$

where E_j and E_r are Young's modulus of fracture and rock matrix element, respectively. k_n is the normal stiffness of fracture. b is mean size of fracture element. In the present work, mean size of fracture element is defined as the square root of cell element area, i.e.,

$$b = \sqrt{S}, \tag{14}$$

where S is the area of fracture element and it can be expressed as,

$$S = \iint |J| \mathrm{d}\xi \mathrm{d}\eta, \tag{15}$$

where, J is the Jacobi matrix, and ξ, η are the local coordinates of the element.

Equation 13 originates from calculation of equivalent properties in fractured rock domain (see Ruqvist and

Stephansson 2003), but was modified for an approximate representation of the equivalent softening effect of a fracture intersecting a continuum element.

For a weak element, the residual permeability k_r for fracture elements reflects the permeability increase by an intersecting fracture. The k_r value in eq. 11 was calculated as

$$k_r = \frac{e_r^3}{12b} \tag{16}$$

where e_r is the residual fracture aperture at high compressive stress and b is the mean size of fracture elements.

The parameters used in the simulation for elastic and elasto-plastic analysis were listed in Table 1.

In elasto-visco-plastic analysis, the determination of parameters c and φ is based on the shear creep test results on hard saturated fracture with no filling from test results for the three Gorges Project by Ding (2005).

The mechanical behavior of the fractures under constant shear stress can be described by the elasto-visco-plastic model, whose visco-plastic parameters Γ and N are obtained based on the shear creep strain in the shear creep tests. Its procedure is the same as Desai Chandre et al. (1995), which has been detailed in the procedures of the intact rock (granite).

Based on the work earlier, the parameters for elasto-visco-plastic analysis are tabulated in Table 2. More details in obtaining the visco-plastic parameters can be found in the report by Feng et al. (2006b).

Coupled THM evolution behavior in EDZ

Linear elastic THM solutions

In linear elastic and elasto-plastic analysis, the parameters were shown in Table 1. It should be noted that Young's modulus of fracture elements were calculated automatically using Eq. 13 because fracture elements' mean size is different from each other.

The elastic THM solutions of WB2 were performed by using three fracture models at 100 years (Fig. 4), in which the results by using conventional Goodman element (GJE1) agree well with the results from other research teams of DECOVALEX-THMC Task B (Rutqvist et al. 2006b). As
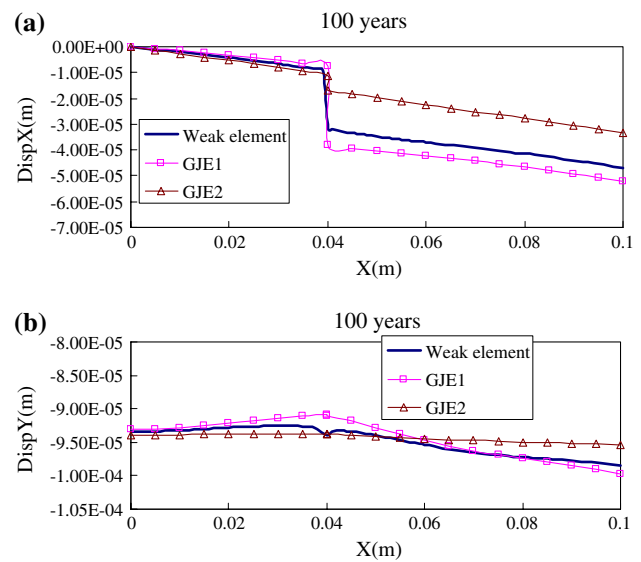

Fig. 4 Profiles of x and y displacement along wall surface $y = 0.0$ at 100 years for WB2. **a** Displacement X. **b** Displacement Y

the GJE2 considers a nonlinear relation between normal stress and normal displacement, smaller displacement occurs at the place near fracture elements. Furthermore, the stress concentration is more localized by using GJE2 than that of using GJE1 and weak element as fracture representations (Fig. 5). The results of Figs. 4 and 5 also indicate the feasibility and reasonability of using weak element as fracture representation, as they show the same trend in the THM evolutions of wall block model domains. However, as mentioned above, the weak element is treated as an isotropic material, which causes some difference in results between using weak element and the conventional Goodman element. The anisotropic property of weak elements can also be considered. This can be developed in the numerical realizations to solve models with a few fractures, whose geometric properties (including fracture dip angle, fracture length, etc.) can be easily measured. However, if the model contains a complex fracture network (Fig. 1b), the implementation of anisotropic properties will be difficult for determination of the fracture network geometry. From the results shown in Figs. 4 and 5, it can be found that the weak element is suitable for modeling the mechanical behavior and permeability variation of fracture network model in the EDZ.

Table 2 The viscoplastic parameters of the intact rock matrix and the fractures in its tangential direction

|	Cohesion c (MPa)	Angle of internal friction ϕ	Fluidity parameter Γ	Power parameter N	Tensile strength σ_t (MPa)
Intact rock	29.0101	41.5466°	8.3941E-9	0.8451	14.8
Fracture	0.01944	35.5476°	5.7819E-11	0.2935	0
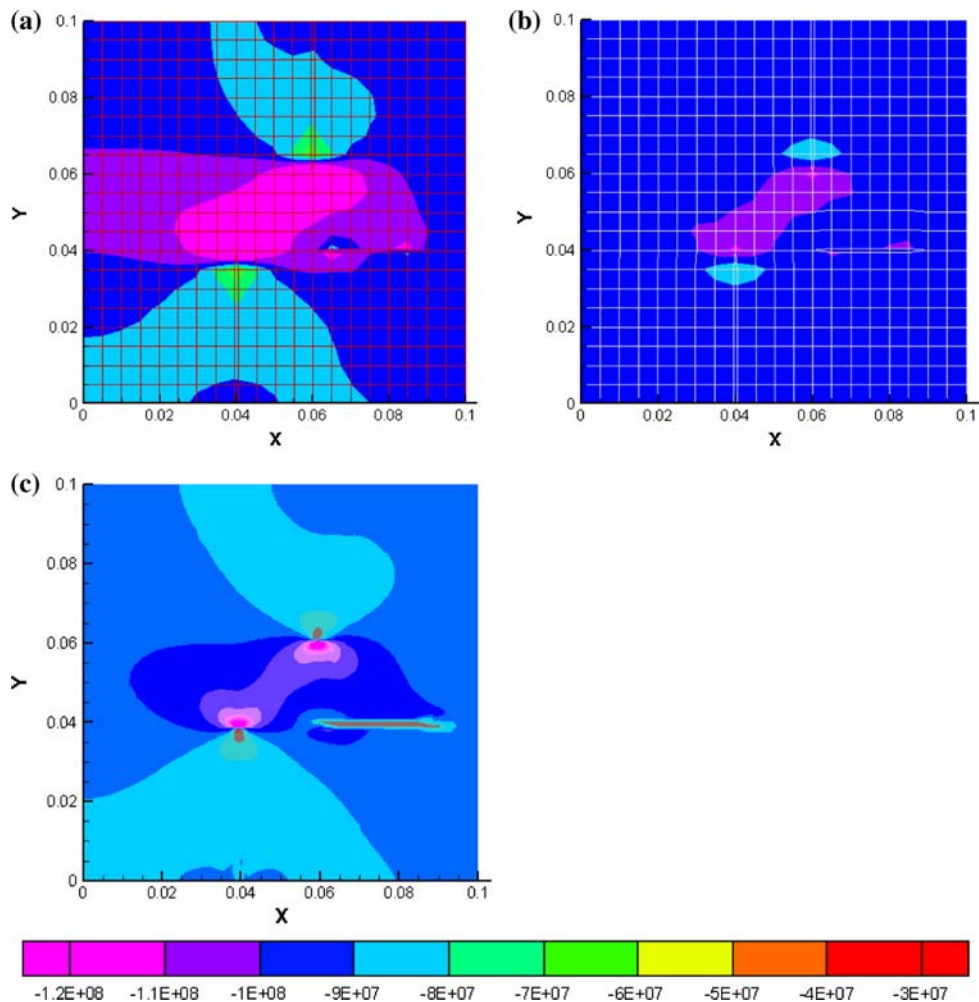
For the simulation of near-field model domains shown in Fig. 1b, the homogeneous NF model was firstly discretized into a grid (or cell) system composed of cell elements, followed by covering the fracture pattern Fig. on the grid system of homogeneous NF model and identifying the cell elements intersected by the fractures. These cell elements were coined as weak elements whose physical properties are much weaker than intact rock matrix elements, with lower Young's modulus and strength of weak elements, but higher permeability. By using this method, heterogeneous stress and permeability distributions of near-field fracture network model were well represented, comparing with that of homogeneous NF model domain (Fig. 6). It can be seen that at places where the fracture intersected, stress concentration and permeability increase are more significant. At the top of the drift, compressive stress state dominates this area and the volumetric strain is always in contraction. The compressive stress near the top drift wall is largest, but reduced upwards towards the top surface of the model. Therefore, permeability increases with the increase of the vertical distance from the tunnel wall upwards.
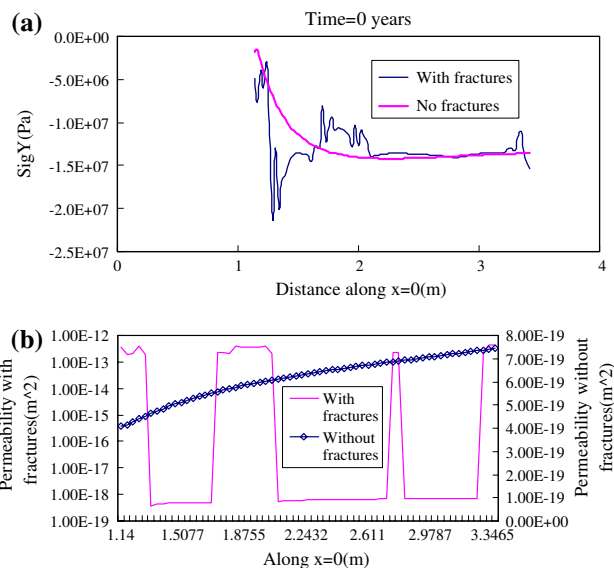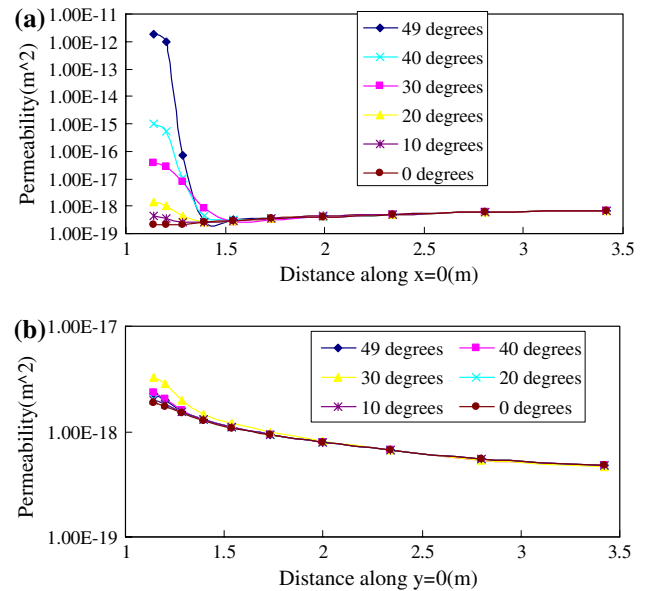

Fig. 6 Profiles of stress and permeability along *y*-axis of NF models with and without fractures at excavation. **a** Stress. **b** Permeability
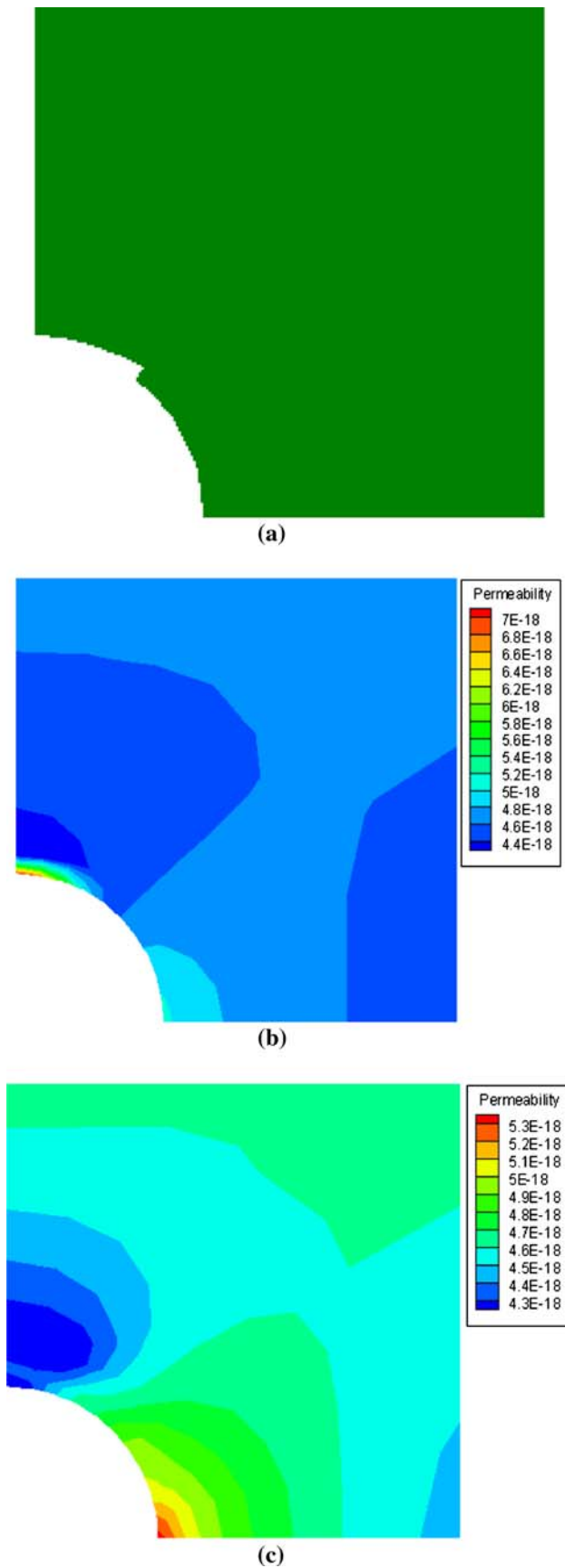
(a)

(b)

(c)

Fig. 8 Permeability profiles at excavation with different dilation angles. **a** Distance along $x = 0$. **b** Distance along $y = 0$
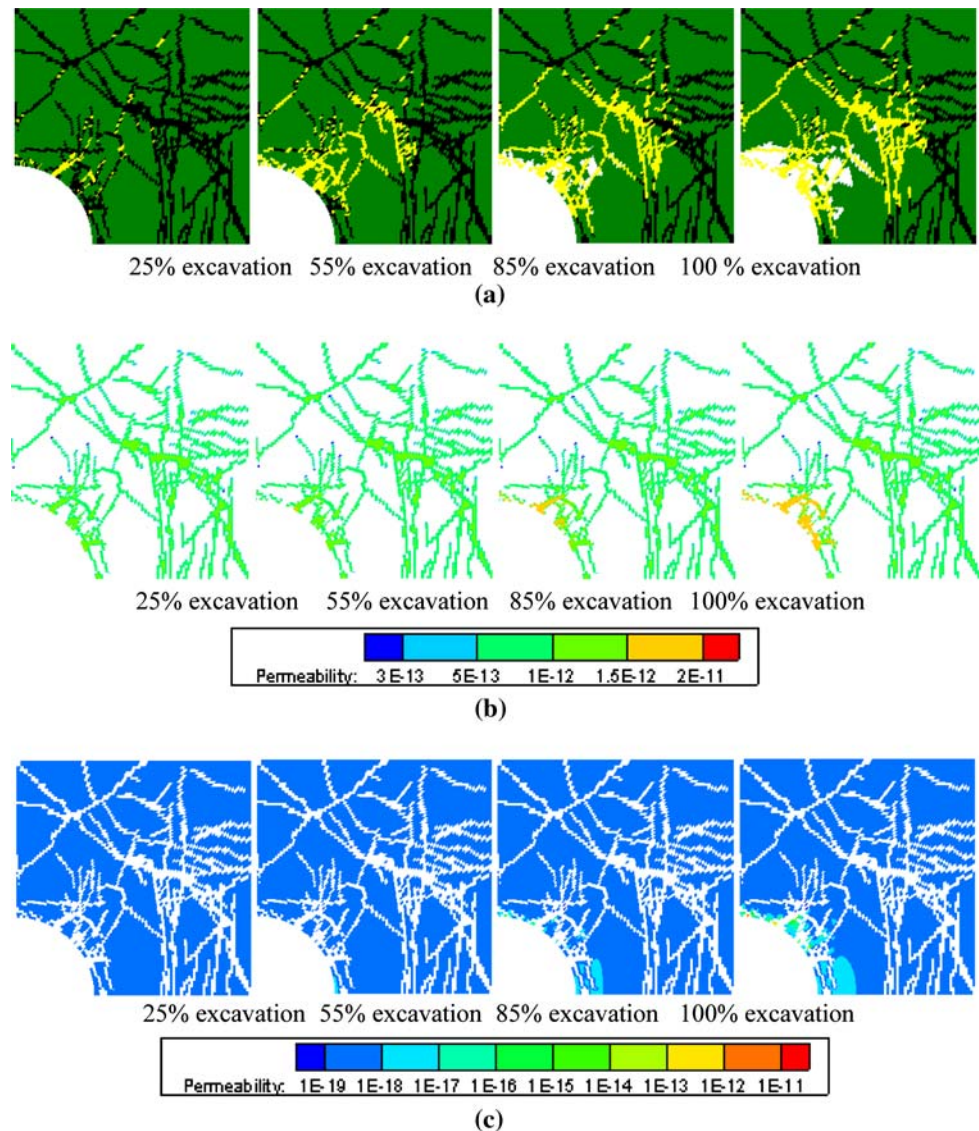
Non linear/elasto-plastic failure analysis

Elasto-plastic failure analyses were conducted in wall block and near-field model domains. This study concentrated on the stress redistribution caused by opening of the tunnel and the effect of this stress redistribution on the fractures and rock matrix systems. An initial stress state of 13.2 MPa in the vertical direction and 32.1 MPa in the horizontal direction was assigned to the model. The radial stress on drift wall is released step by step until the stress at drift wall becomes 0. In the simulation, at each step, the unloading rate is 1%. Therefore, at step 100, the boundary stress at drift wall is 0, indicating the completion of the drift excavation.

For the homogenous near-field model, failure zones are found at the roof of the drift when different dilation angles are adopted (Fig. 7a). The permeability variations are shown in Fig. 7b and c. It can be found that, due to the shear dilation, permeability increases significantly at the roof of the drift (Fig. 7b). When dilation angle is 0, the permeability seems not influenced by the failure of rock mass and the maximum permeability was found at the spring line of the drift (Fig. 7c).

Figure 8 is the permeability profiles along $x = 0$ and $y = 0$ at the completion of drift excavation with different dilation angles. The influence of shear dilation on the permeability distribution is significant at the top of the

Fig. 9 a Failure process. **b** Permeability variation of rock matrix. **c** Permeability variation of fracture system of near-field fracture network model domain by unloading radial stress stepwise at drift wall with different dilation angle with dilation angle 49° at rock matrix and 27° at fracture

25% excavation   55% excavation   85% excavation   100 % excavation
(a)

25% excavation   55% excavation   85% excavation   100% excavation

Permeability: 3E-13   5E-13   1E-12   1.5E-12   2E-11
(b)

25% excavation   55% excavation   85% excavation   100% excavation

Permeability: 1E-19 1E-18 1E-17 1E-16 1E-15 1E-14 1E-13 1E-12 1E-11
(c)

tunnel because of shear failure at this place (Fig. 8a). At the springline, as there is no failure occurs, dilation angle has no obvious effect on the permeability change (Fig. 8b).

Fig. 9a shows the failure process of near-field fracture network domain. The failure processes are influenced by fractures significantly. In the excavation process, not all the fractures are failed by shear. Rock matrix failure occurs when the stress around the drift is released to a very low level. The failure processes and the associated permeability variation are shown in Fig. 9b and c.

In real situations, the dilation angle can be much lower than frictional angle for crystalline rocks. In the simulations, different magnitude of frictional angle is used to study the difference of using associated and non-associated plastic flow rules, as a parameter sensitivity analysis.

Time-dependent creep analysis

The rock mass begins to creep right after linear elastic deformation completed. In this study, Nishihara model and modified Goodman Element (GJE3, Fig. 3c) model were used to describe the creep behavior of rock matrix and fracture, respectively, with consideration of THM effect. In the simulation, constant bulk modulus was assumed, which means that only shear deformation was influenced by the visco-elastic behavior, while the volumetric deformation is elastic during the creep process. The visco-plastic parameters of intact rock matrix and fracture are shown in Table 2.

Creep analysis was conducted at different stress levels with a time scale from the completion of drift excavation to 1e6 years, which was divided into a number of loading steps. At each step, the model will be run until a steady
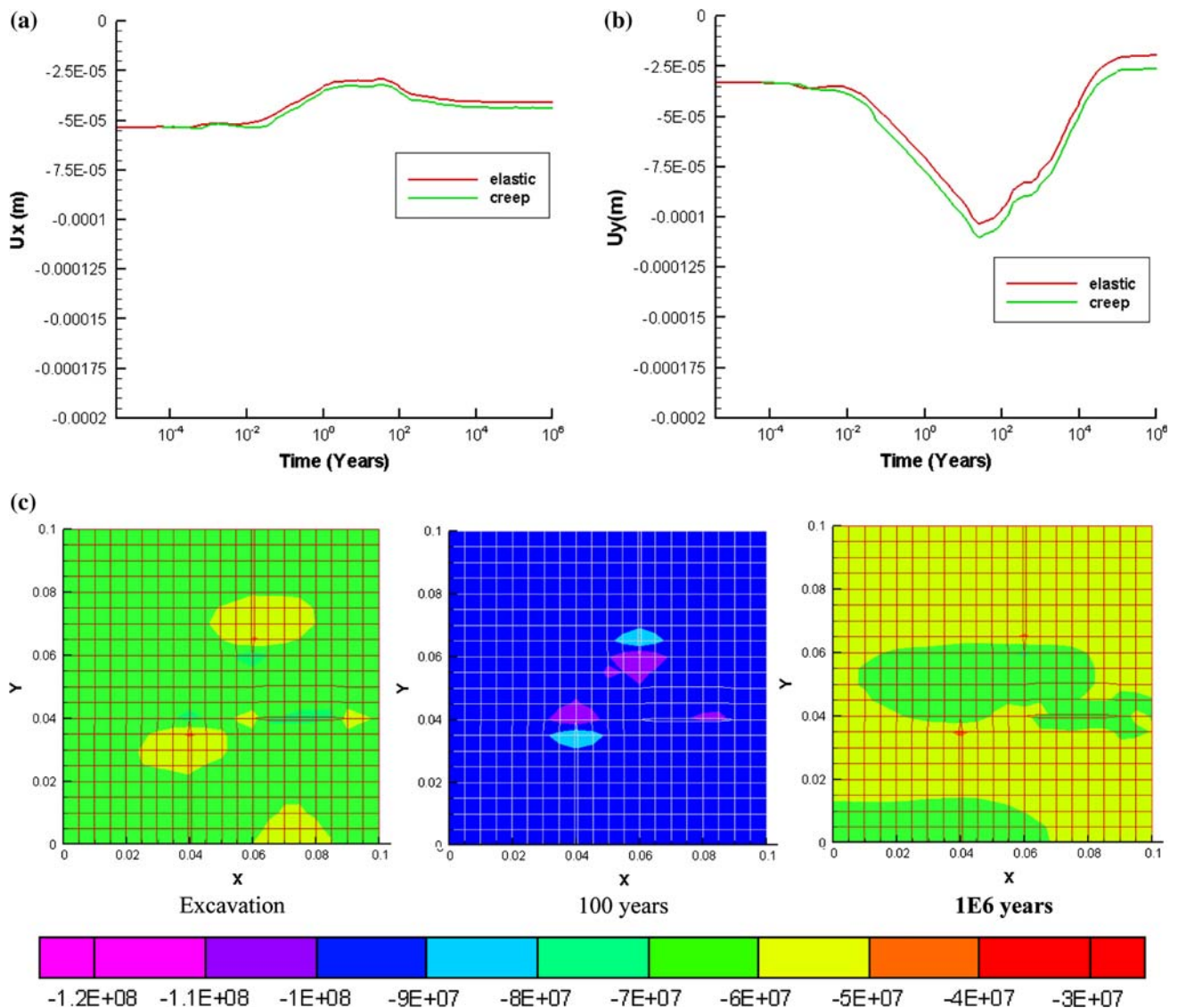
Fig. 10 **a** Time evolution of X-displacement. **b** Y-displacement at the corner (0.1,0.0) with and without consideration of creep. **c** Minimum principal stresses at excavation, 100 years and 1e6 years for the wall block Model 2

creeping is reached. Afterwards, the loading started again for the next step. At steady creep state, the magnitude of visco-elastic strain and visco-plastic strain rates of current load step was reduced to a specific value. If an element cannot reach a steady creep within the prescribed iteration process, the residual visco-elastic and visco-plastic strain rates will be transformed into equivalent nodal force as the unbalanced force of current time step. This unbalanced force, together with the load of next step, will be subjected to the model in the creep of next load step.

Figure 10a and b compare time evolutions of X- and Y-displacements at the lower left corner (0.1, 0.0) of the wall block model 2 with and without consideration of creep. Due to the opening of horizontal fracture, creep deformation occurs mainly in the two vertical fractures. The change

of Y-displacement is more than that of X-displacement, comparing with the elastic results without creep.

Creep analysis indicated that the principal stress distribution of WB0 and WB1 models have no difference between creep analysis and elastic analysis. However, for WB2 with no intersected fractures, significant stress concentration was found around the fractures in elastic analysis. At the end of elastic analysis, the change of inhomogeneous stress distribution continues after the creep analysis follows. Figure 10c shows the minimum principal stress distribution in WB2 model, at the end of excavation 100 and 1e6 years, respectively. Comparing with the results of elastic analysis (Fig. 5), the stress concentration zones were reduced further when creep analysis was stable at 100 years. According to the elasto-visco-plastic constitutive relation of fractures, the stress

exceeded the yield strength will be released continually and re-assigned to the neighbouring rock matrix. The extent of stress concentration around fractures was relaxed.

Conclusions

This paper presents analyses of the coupled THM processes in the EDZ of crystalline rocks by CAS research team using EPCA code. Numerical results indicate a strong impact of fractures and shear dilation of rock matrix on the distribution of rock stress and deformation, which in turn affects the evolution of failure and permeability around the drift.

The analysis conducted in this study shows the importance of the small-scale heterogeneity, which lead to enhanced stress concentration that in turn leads to additional failure. In a homogeneous continuum model such stress concentrations could be smoothed out and failure may be less extensive. The results in this study were obtained for considering one fracture mapping data extracted from the tunnel walls at the Äspö Hard Rock Laboratory. Thus, this is specific representation of a "real" fracture network. The results for a similar fracture pattern would most likely show similar general behavior, i.e. stress redistribution around fractures and most failure in the zones of the highest shear stress (above the drift). However, the magnitude and exact location of the largest stress and permeability changes will depend on where and at what angle fractures intersect the tunnel wall for one particular fracture pattern. Thus, for estimating the evolution of the excavation disturbed zone at a future site for high level nuclear waste, this type of analysis should be conducted using many realizations of the fracture patterns, leading to statistical distributions of likely failure and permeability changes.

Different fracture models were used to represent fractures in fractured wall block and near-field fracture network models. The weak element technique may be much more realistic when the models contain fracture networks. In the paper, the anisotropic properties of fractures were not considered. Although isotropic elastic and elasto-plastic models were applied, anisotropic fracture deformation behavior can still be achieved, because most substantial shear and normal deformation will automatically tend to occur, respectively, along and normal to the trace of weak fracture elements.

Parameter determination is very important in numerical simulations. DECOVALEX-THMC Task B does not and cannot provide all the parameters for simulations because different numerical model/tool requires different input data. In this paper, some of the data (for example, elasto-visco-plastic parameters) came from literature study and some came from Task B. Other data such as cellular automaton iterative precision is assumed according to the requirement of EPCA model.

The models are in two dimensions in the reported study. In future, fracture characteristics and modeling under 3D conditions will be considered.

References

Bäckström A (2006) Obtaining the fracture pattern to use in the near field model 2 in phase 3 in Task B in the DECOVALEX IV Cooperation

Bäckström A, Antikainen J, Backers T, Feng X-T, Jing L, Kobayashi A, Koyama T, Pan P-Z, Rinne M, Shen B, Hudson JA (2008) Numerical modelling of uniaxial compressive failure of granite with and without saline pore water. Int J Rock Mech Min Sci 43:1091–1108

Desai Chandre S, Samtani Naresh C, Vulliet L (1995) Constitutive modeling and analysis of creeping slopes. J Geotech Eng 121(1):43–56

Ding X-L (2005) Experimental study on rock mass rheological properties and identification for the constitutive model and parameters. Ph.D., Institute of Rock and Soil Mechanics, the Chinese Academy of Sciences, China [in Chinese]

Elsworth D (2003) Some THMC controls on the evolution of fracture permeability. In: Stephansson O, Hudson JA, Jing L (eds) Coupled Thermo-hydro-mechanical-chemical processes in geo-systems, Proc Int Conf GeoProc2003. Stockholm, pp 63–71

Elsworth D, Yasuhara H (2006) Short-mimescale chemo-mechanical effects and their influence on the transport properties of fractured rock. Pure Appl Geophys 163:2051–2070

Feng XT, Chen SL, Li SJ (2001) Effects of water chemistry on microcracking and compressive strength of granite. Int J Rock Mech and Min Sci 38(4):557–568

Feng XT, Li SJ, Chen SL (2004) Effect of water chemical corrosion on strength and cracking characteristics of rocks-a review. Key Eng Mater 261–263:1355–1360

Feng XT, Pan PZ, Zhou H (2006a) Simulation of rock microfracturing process under uniaxial compression using elasto-plastic cellular automata. Int J Rock Mech and Min Sci 43:1091–1108

Feng X-T, Huang X-H, Pan P-Z (2006b) DECOVALEX THMC Task B, phase 3 stage 3: time dependent failure modelling, extend model for analysis of creep and mechanical degradation, Initial modeling results by the CAS research team[R]. Chinese Academy of Sciences, May 20

Hart RD, John CMST (1986) Formulation of a fully-coupled thermal-mechanical-fluid model for non-linear geologic systems [J]. Int J Rock Mech Min Sic Geomech Abstr 23(3):213–224

Hudson JA, Christiansson R (2006) Studying coupled effects in the excavation disturbed zone (EDZ) for a crystalline rock: the work of DECOVALEX-THMC Task B. In: Xu W-Y (ed) The 2nd international conference on coupled T-H-M-C processes in geo-systems, Proc Int Conf GeoProc2006. Hohai University, pp 108–117

Hudson JA, Stephansson O, Andersson J (2005) Guidance on numerical modelling of thermo-hydro-mechanical coupled processes for performance assessment of radioactive waste repositories. Int J Rock Mech Min Sci 42(5–6):850–870

Hudson JA, Bäckström A, Rutqvist J, Jing L, Backers T, Chijimatsu M, Feng X-T, Kobayashi A, Koyama T, Lee H–S, Pan P-Z, Rinne M, Shen B (2008) Characterization and modeling the excavation damaged zone (EDZ) in crystalline rock in the context of radioactive waste disposal. Environ Geol (this issue)

Jing L, Feng X-T (2003) Numerical modeling for coupled thermo-hydro-mechanical and chemical processes (THMC) of geological media–international and Chinese experiences[J]. Chin J Rock Mech Eng 22(10):1704–1715

Lewis RW, Schrefler BA (1987) The finite element method in deformation and consolidation of porous media. Wiley, New York

Liu J, Sheng J, Polak A, Elsworth D, Yasuhara H, Grader A (2006) A fully-coupled hydro- mechanical- chemical model for fracture sealing and preferential opening. Int J Rock Mech Min Sci 43(1):23–36

Nguyen T-S, Selvadurai APS (1995) Coupled thermal-mechanical-hydrological behaviour of sparsely fractured rock:implications for nuclear, fuel waste disposal. Int J Rock Mech Min Sic Geomech Abstr 32(5):465–479

Noorishad J, Tsang C-F (1996) ROCMAS-simulator: a thermohydro-mechanical computer code. In: Stephansson O, Jing L, Tsang C–F (eds) Coupled thermo-hydro-mechanical processes of fractured media. Developments in geotechnical engineering, Elsevier, 79, pp 551–558

Noorishad J, Tsang C-F, Witherspoon PA (1984) Coupled thermal-hydraulic- mechanical phenomena in saturated fractured porous rocks: numerical approach. J Geophysical Res 89(B12):10365–10373

Ohnishi Y, Shibata H, Kobayashi A (1987) Development of finite element code for the analysis of coupled thermo-hydro-mechanical behavior of a saturated-unsaturated medium. In: Tsang C-F (ed) Proceedings of international symposium on coupled process affecting the performance of a nuclear waste repository, Berkeley, pp 551–557

Pan P-Z, Feng X-T, Hudson JA (2006a) Simulations on Class I and Class II curves by using the linear combination of stress and strain control method and elasto-plastic cellular automata. Int J Rock Mech and Min Sci 43:1109–1117

Pan P-Z, Feng X-T, Zhou H (2006b) Simulation of rock fracturing in an HM coupling environment using a cellular automaton. In: Xu W-Y (ed) The 2nd international conference on coupled T-H-M-C processes in geo-systems, Proc Int Conf GeoProc2006. Hohai University, pp 503–508

Polak A, Yasuhara H, Elsworth D, Liu J, Grader A, Hallek P (2004) The evolution of permeability in natural fractures—the competing roles of pressure solution and free-face dissolution. In: Stephansson O , Hudson JA, Jing L (eds) Coupled thermo-hydro- mechanical-chemical processes in geo-systems, Proc Int Conf GeoProc2003, Stockholm, p 721–726

Ruqvist J, Stephansson O (2003) The role of hydromechanical coupling in fractured rock engineering. Hydrogeol J 11:7–40

Rutqvist J (2007) SKI/LBNL's modeling of Task A2 using ROCMAS code. In: Nguyen TS, Lanru J (eds) DECOVALEX-THMC Project Task A "Influence of near-field coupled THM phenomena on the performance of a spent fuel repository" (Chapter 4), Report of Task A2, DECOVALEX SKI Report

Rutqvist J, Börgesson L, Chijimatsu M, Kobayashi A, Nguyen T-S, Jing L, Noorishad J, Tsang C-F (2001) Thermohydromechanics of partially saturated geological media—governing equations and formulation of four finite element models. Int J Rock Mech Min Sci 38:105–127

Rutqvist J, Wu Y-S, Tsang C-F, Bodvarsson G (2002) A modeling approach for analysis of coupled multiphase fluid flow, heat transfer, and deformation in fractured porous rock. Int J Rock Mech Min Sci 39:429–442

Rutqvist J, Sonnenthal E, Jing L, Hudson J (2006a) Task definition for DECOVALEX THMC Task B, Phase 3: a bench mark test on drift wall coupled THMC processes

Rutqvist J, Feng X-T, Hudson J, Jing L, Kobayashi A, Koyama T, Pan P-Z, Lee H S, Rinne M, Sonnenthal E, Yamamoto Y (2006b) Multiple-code benchmark simulation study of coupled THMC processes in the excavation disturbed zone associated with geological nuclear waste repositories. In: Xu WY (ed) The 2nd international conference on coupled T-H-M-C processes in geo-systems, Proc Int Conf GeoProc2003. Hohai University, pp 397–402

Rutqvist J, Bäckström A, Chijimatsu M, Feng X-T, Pan P-Z, Hudson JA, Jing L, Kobayashi A, Koyama T, Lee HS, Huang X-H, Rinne M, Shen B (2008a) A bench mark simulation study of the long-term EDZ evolution of geological nuclear waste repositories. Environ Geol (this issue)

Rutqvist J, Barr D, Birkholzer JT, Fujisaki K, Kolditz O, Liu Q-S, Fujita T, Wang W, Zhang C-Y (2008b) A comparative simulation study of coupled THM processes and their effect on fractured rock permeability around nuclear waste repositories. Environ Geol (this issue)

Rutqvist J, Börgesson L, Chijimatsu M, Hernelind J, Jing L, Kobayashi A, Nguyen T-S (2008c) Modeling of damage, permeability changes and pressure responses during excvation of the TSX tunnel in granitic rock at URL, Canada. Environ Geol (this issue)

Shen B, Stephansson O (1993) Numerical analysis of mixed mode-I and mode-II fracture propagation. Int J Rock Mech Min Sci 30:861–867

Stephansson O, Jing L, Hudson JA (eds) (1996) Coupled T-H-M-C processes of fractured media. Devel Geotech Eng 79, Elsevier, Amsterdam

Stephansson O, Jing L, Hudson JA (eds) (2004) Coupled T-H-M-C processes in geosystems: fundamentals, modeling, experiment and applications, Elsevier, Oxford

Tsang C-F (ed) (1987) Coupled processes associated with nuclear waste repositories. Academic Press, New York

Tsang C-F, Stephansson O, Jing L, Kautsky F (2008) An overview of the DECOVALEX project 1992–2007. Environ Geol (this issue)

Yasuhara H, Elsworth D (2006a) A numerical model simulating reactive transport and evolution of fracture permeability. Int J Numer Anal Meth Geomech 30:1039–1062

Yasuhara H, Elsworth D (2006b) A numerical model simulating evolution of fracture permeability moderated by mechanically- and chemically-induced dissolution. In: Xu W-Y (ed) The 2nd international conference on coupled T-H-M-C processes in geo-systems, Proc Int Conf GeoProc2003. Hohai University, pp 338–343